Journal of the Korean Physical Society (2025) 86:806–818
https://doi.org/10.1007/s40042-025-01319-4

Online ISSN 1976-8524
Print ISSN 0374-4884

RESEARCH - CROSS-DISCIPLINARY PHYSICS AND RELATED AREAS OF SCIENCE AND TECHNOLOGY

Feasibility of 3D quality assurance system with electrode array for electric fields therapy

Jinyoung Hong[1] · Yunhui Jo[2] · Yongha Gi[1] · Geon Oh[1] · Hyeongjin Lim[1] · Yousun Ko[1] · Sung Hwan Ahn[4] · Myonggeun Yoon[1,3]

Received: 5 November 2024 / Revised: 21 January 2025 / Accepted: 11 February 2025 / Published online: 21 February 2025

Abstract

In this study, we investigated the feasibility of a three-dimensional quality assurance system for Tumor-Treating Fields (TTFields) therapy by applying voltage to a water phantom using an electrode array. The water phantom was prepared by mixing deionized (DI) water with NaCl. A voltage of 50 V_{pp} at 150 kHz was applied to the phantom, and voltage measurements were taken along five profiles by moving the probe within the phantom to minimize electric field distortion. The experimental data were analyzed using error rates and gamma index analysis. In the three-dimensional evaluation, the average differences in voltage and electric field were 1.06% and 6.65%, respectively. The gamma passing rates for voltage, using criteria of 5%/3 mm and 3%/3 mm, were 100% and 99.61%, respectively. For the electric field, the gamma passing rates were 93.63% and 88.31% when evaluated using criteria of 10%/5 mm and 5%/5 mm, respectively. These findings suggest that employing three-dimensional quality assurance with the electrode array can significantly enhance the treatment quality of TTFields therapy.

Keywords Quality assurance · Phantom · Electric fields therapy · Tumor-treating fields

1 Introduction

Electric fields for cancer treatment, also known as Tumor-treating fields (TTFields), represent a novel approach that uses low-intensity electric fields (*E*-field) at intermediate frequencies (100–300 kHz) [1–3]. This therapy has been approved by the U.S. Food and Drug Administration for the treatment of glioblastoma and mesothelioma [3, 4]. Additionally, TTFields is widely utilized in clinical trials and research targeting various cancers, including non-small-cell lung cancer, pancreatic cancer, and liver cancer [5–7]. Ongoing research continues to explore the efficacy of TTFields in combination with other treatment modalities, such as radiotherapy and chemotherapy [8–10].

TTFields therapy works by disrupting cell division through the application of an induced *E*-field in the cells, ultimately leading to cell death [2, 11, 12]. Two mechanisms are recognized as integral to its therapeutic effect. First, induced electric fields (*E*-fields) interfere with the assembly of mitotic spindles [2, 12]. Second, irregular *E*-fields, arising from structural disparities in cells during cytokinesis induce cell death [2, 12]. Among the two treatment mechanisms associated with TTFields, the principal mechanism is presumed to be dielectrophoresis occurring in cells during telophase [12, 13]. The magnitude of this dielectrophoresis appears to be directly proportional to the square of the *E*-field intensity, which has been reported to affect treatment efficacy [1, 11, 13, 14]. Therefore, accurately understanding the magnitude of the *E*-fields induced within the body is critical for enhancing the efficacy and quality of *E*-field-based therapies.

✉ Sung Hwan Ahn
sung.hwan.ahn@samsung.com

✉ Myonggeun Yoon
radioyoon@korea.ac.kr

1 Department of Bio-Medical Engineering, Korea University, Anamro 145, Seongbuk-gu, Seoul 02842, Republic of Korea

2 Institute of Global Health Technology (IGHT), Korea University, Seoul, Republic of Korea

3 FieldCure Ltd, Seoul, Republic of Korea

4 Department of Radiation Oncology, Samsung Medical Center, Seoul, Republic of Korea

In radiotherapy (RT), quality assurance (QA) procedures are essential to ensure treatment accuracy and safety. This therapy requires the precise delivery of radiation doses and accurate patient positioning, as any deviations could compromise treatment efficacy and increase the risk of side effects or serious medical incidents. To address this, QA procedures involve measuring the radiation dose distribution before treatment and comparing it with the planned distribution [15–17]. Various techniques are used to measure radiation dose distribution in RT, including point (1D), two-dimensional (2D), and three-dimensional (3D) QA methods. To enable more precise and sophisticated treatments, ongoing research focuses on developing advanced methodologies and technologies for 3D dose distribution measurement. The significance of 3D dosimetry continues to grow in the field [18–20].

Unlike in radiotherapy (RT), where 3D QA systems have been developed, no such systems have been proposed for TTFields therapy, which involves three-dimensional *E*-field distributions within the body. To date, only one-dimensional (1D) and two-dimensional (2D) QA systems using single electrode pairs have been introduced [21, 22]. However, validating the 3D spatial distribution of voltage and *E*-fields is crucial for accurately assessing treatment efficacy. Therefore, accurately measuring the 3D *E*-field distribution is essential for more precise treatment validation. In actual treatments, electrode arrays are used, which complicates the current density distribution. Due to the edge current effect, a single electrode produces uneven current density. Electrode arrays, in turn, generate even more complex current density patterns depending on their configuration [23, 24]. This nonuniform current density leads to uneven *E*-field distributions as governed by Ohm's law, increasing uncertainty in predicting treatment outcomes and potential side effects [24, 25]. Consequently, there is a clear need for a 3D QA system designed specifically to accommodate electrode arrays.

In this study, we assessed the feasibility of a 3D QA system by applying voltage to a water phantom using a pair of electrode arrays consisting of four electrodes. The measured voltage and the *E*-field distributions were compared with reference values calculated using the finite element method in one, two, and three dimensions. Additionally, the QA system was evaluated using error rates and gamma index analysis.

2 Methods

2.1 Experimental setup

A water phantom was designed to replicate the electrical conductivity of muscle tissue, targeted at 0.367 S/m, which corresponds to the conductivity of muscle at 150 kHz [26]. To achieve this, a solution was prepared by mixing 1.35 L of deionized water with 2.1 g of NaCl, resulting in a conductivity of 0.367 ± 0.1 S/m. The water was contained within an acrylic container with inner dimensions of $100 \times 100 \times 150$ mm^3. The container was fitted with a printed circuit board (PCB) to facilitate the attachment of external electrodes (Fig. 1(a)). Copper electrodes with dimensions of $32 \times 22 \times 1$ mm^3 were affixed to the water phantom using medical-grade hydrogel (HUREV; conductivity $\sigma = 0.1$ S/m, relative permittivity $\varepsilon_r = 80$) (Fig. 1(b)). A custom-built generator was used to apply a voltage of 50 V_{pp} at a frequency of 150 kHz across the entire QA system.

The voltage distribution was measured using an oscilloscope (TBS 1102B, Tektronix, OR, USA) and a differential probe (N2791A, Keysight, CA, USA). For the measurements, the "*N*" terminal of the differential probe was connected to the ground electrode, while the "P" terminal was connected to a coaxial cable to minimize noise. Voltage measurements were conducted at 5 mm intervals along the *x* and *y* axes within a single plane and at 10 mm intervals along the *z*-axis. The electric field is defined as the rate of change of the electric potential, and Eq. (1) conceptually represents the calculation of the electric field in this study.

$$E_i = \frac{V_{interp,i+1} - V_{interp,i-1}}{2\Delta r} \tag{1}$$

E_i, $V_{interp,i+1}$, $V_{interp,\,i-1}$, and Δr represent the electric field at point i, the interpolated voltage at $i+1$, the interpolated voltage at $i-1$, and the distance between points, respectively. The measured voltage distribution was interpolated, and its derivatives with respect to position were calculated to obtain the electric field values. A total of 361 points were measured per plane, and measurements were performed on 5 planes, resulting in a total of 1,805 voltage and electric field data points.

2.2 Simulation

To evaluate the accuracy of the QA system, the reference voltage and the *E*-field distributions were obtained using the AC/DC module of COMSOL Multiphysics, version 6.1(COMSOL Multiphysics, COMSOL, Boston, USA). The simulation geometry mirrored that used in the experiment. The dimensions of the water phantom, PCB, hydrogel and each electrode were set to $100 \times 100 \times 150 mm^3$, $122 \times 86 \times 1 mm^3$, $86 \times 60 \times 1 mm^3$, and $32 \times 22 \times 1 mm^3$, respectively (Fig. 1(c)). The electrical conductivity (σ) set at 0.367, 1×10^{-9}, 0.1 and 5.998×10 S/m, respectively. The relative permittivity (ε_r) values for the materials were set to 8.13, 1, 80 and 1, respectively. The σ values, except for those of the electrodes, were directly measured for the materials used in the experiments, whereas theoretical or ideal ε_r values were used, as they minimally affect the

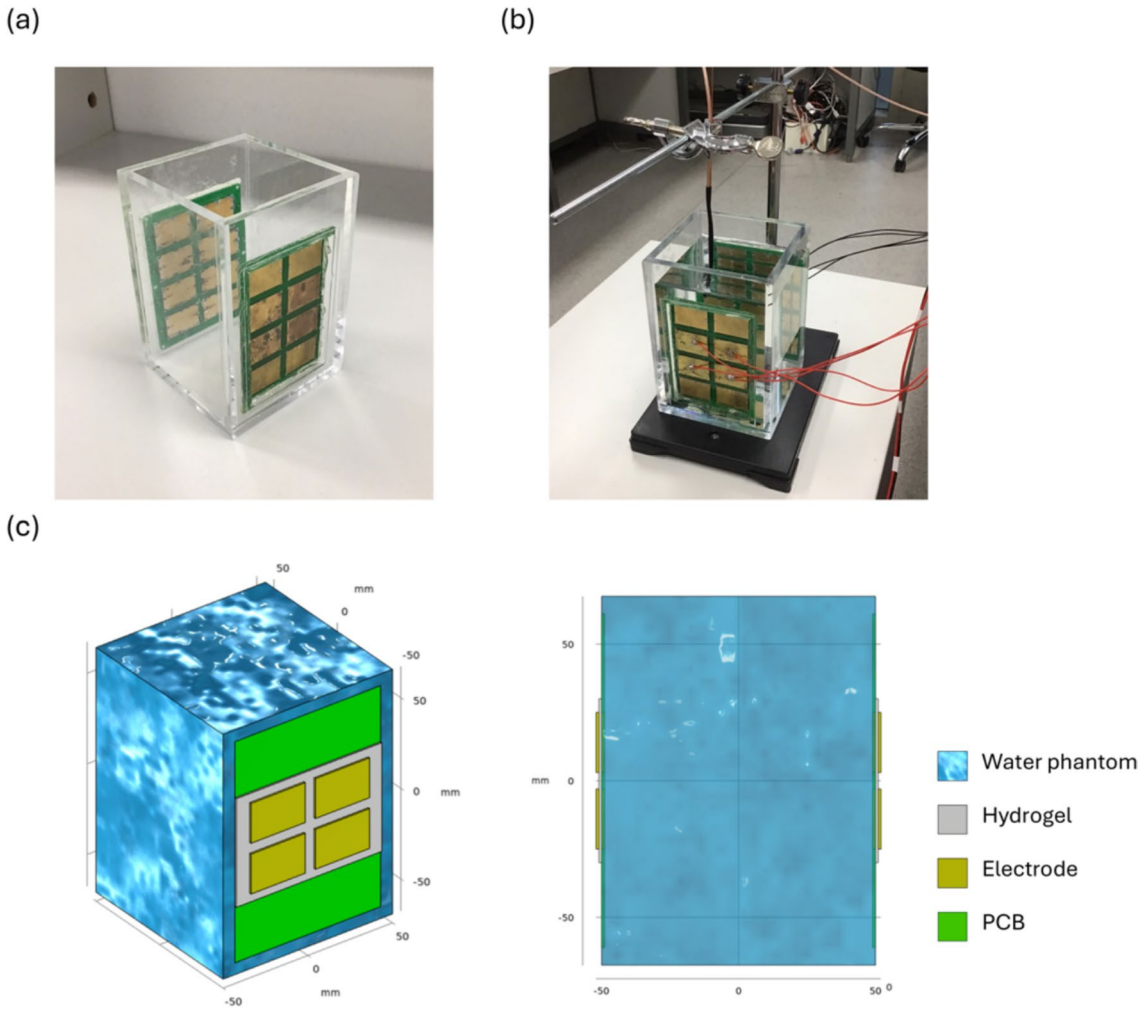

Fig. 1 The experimental setup for measuring voltage and *E*-fields and simulation geometry for calculation. **a** An acrylic container used to contain the water. **b** Four electrode pairs used to apply a voltage to the water phantom. **c** The simulation geometry

E-field distributions [27]. To calculate the *E*-field distribution, all the electrodes attached to one side were designated as ground electrodes, while a voltage of 50 V_{pp} with 150 kHz was applied to the electrodes on the opposite side. The resulting voltage and the electric field distributions were used as reference values.

2.3 Evaluation metrics

To validate the 3D QA system using the water phantom, error rates and gamma index (GI) were calculated at each point. The GI, which simultaneously accounts for both spatial distance and dose differences [28], is commonly used as an evaluation metric in radiation therapy. Equation (2) represents the error rate, which quantifies the discrepancy between the measured value and the reference value. Equations (3) and (4) are used to evaluate the gamma index (GI) for voltage and *E*-fields, respectively.

$$\text{error rate}\,[\%] = \frac{\text{ref}(V,E) - \text{measured}(V,E)}{\text{ref}(V,E)} \times 100 \tag{2}$$

$$GI_{\text{voltage}} = \sqrt{\frac{r^2(r_{\text{ref}}, r_{\text{m}})}{\Delta r^2_{\text{criteria}}} + \frac{V^2(V_{\text{ref}}, V_{\text{m}})}{\Delta V^2_{\text{criteria}}}} \tag{3}$$

$$GI_{\text{E-field}} = \sqrt{\frac{r^2(r_{\text{ref}}, r_{\text{m}})}{\Delta r^2_{\text{criteria}}} + \frac{E^2(E_{\text{ref}}, E_{\text{m}})}{\Delta E^2_{\text{criteria}}}} \tag{4}$$

In these equations, V_{ref}, V_{m}, E_{ref}, and E_{m} represent the voltage reference, the measured voltage, the *E*-field reference, and the measured *E*-field, respectively. The conventional GI equation was modified by replacing the dose term with voltage and *E*-field calculations. For voltage, the dose difference was evaluated using 5% and 3% relative tolerance to the reference at the measurement point, with a distance

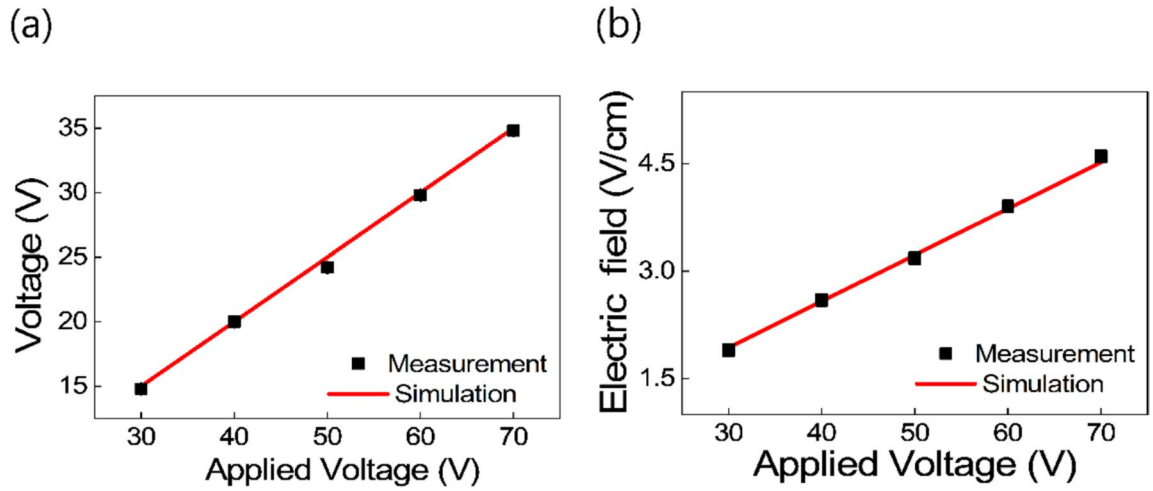

Fig. 2 Voltage and *E*-field linearity depend on the applied voltage at center point. **a** The voltage showing a linear dependence on the applied voltage at the center point. **b** The *E*-field showing a linear dependence on the applied voltage at the center point

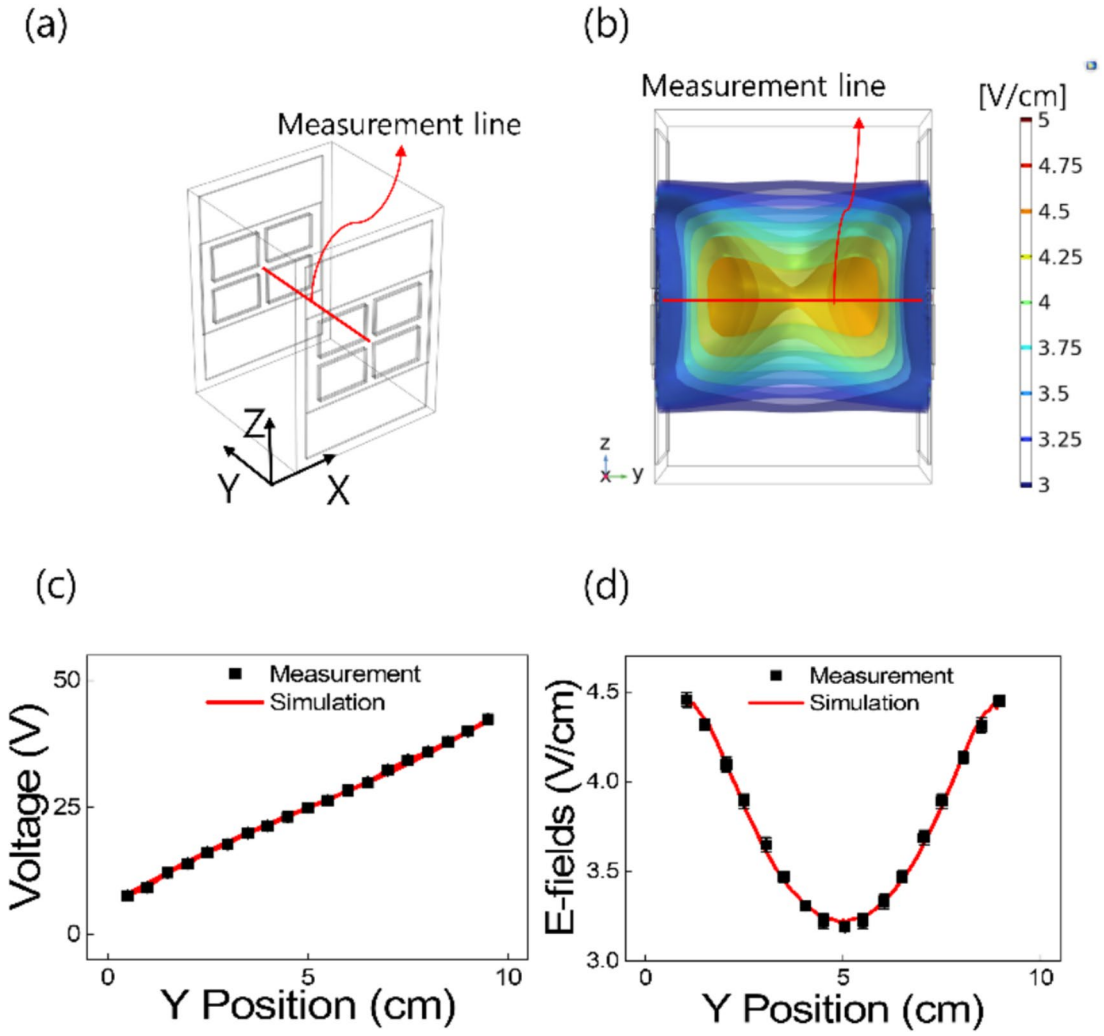

Fig. 3 Voltage and *E*-field distributions in one dimension. **a** Schematic of the measured line. **b** Results of the simulated *E*-field distribution. **c** Voltage distribution on the 1D center line. **d** *E*-field distribution on the 1D center line

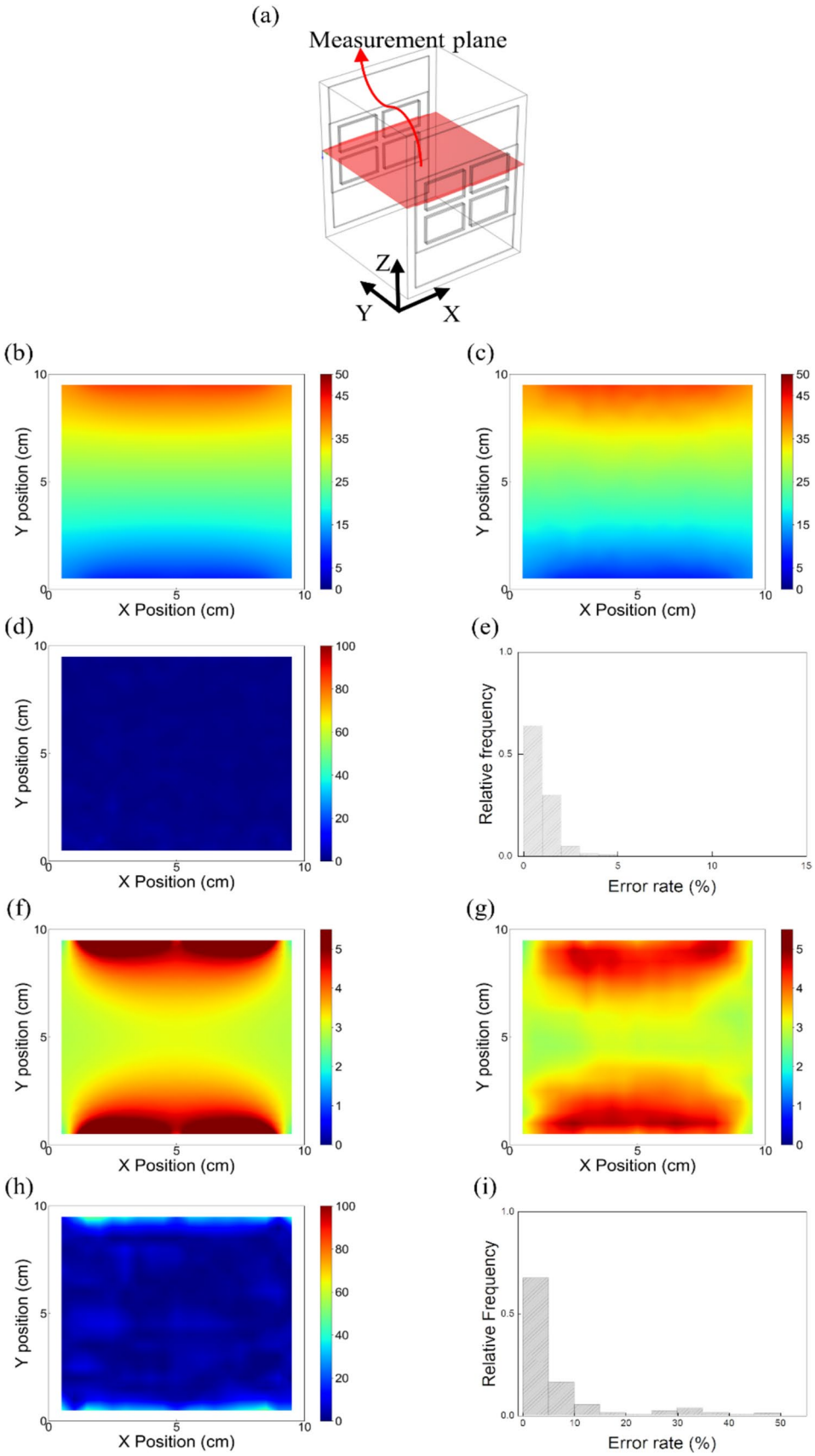

Fig. 4 Voltage and *E*-field distributions at + 10 mm from the center plane. **a** Schematic of the measurement plane. **b** Results of the simulated voltage distribution. **c** Results of the experimental voltage distribution. **d** Error rate between the simulation and experimental voltage distribution results. **e** Histogram of error rate for the voltage distribution. **f** Results of the simulated *E*-field distribution. **g** Results of the experimental *E*-field distribution. **h** Error rate between the simulation and experimental *E*-field distribution results. **i** Histogram of error rate for the E-field distribution

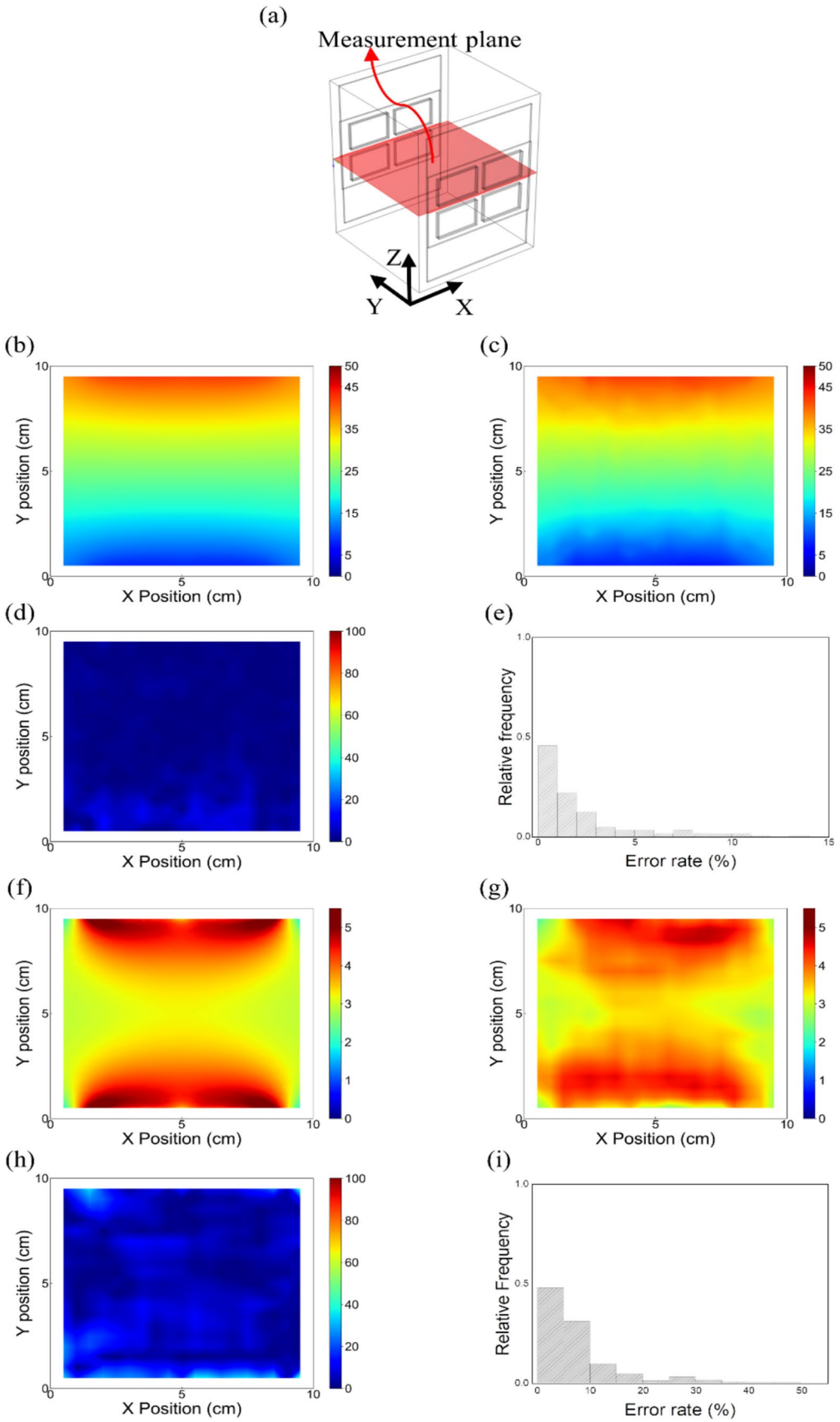
(a)
Measurement plane
Z
Y
X
(b)
Y position (cm)
X Position (cm)
(c)
Y position (cm)
X Position (cm)
(d)
Y position (cm)
X Position (cm)
(e)
Relative frequency
Error rate (%)
(f)
Y position (cm)
X Position (cm)
(g)
Y position (cm)
X Position (cm)
(h)
Y position (cm)
X Position (cm)
(i)
Relative Frequency
Error rate (%)

◂**Fig. 5** Voltage and *E*-field distributions at the center plane. **a** Schematic of the measurement plane. **b** Results of the simulated voltage distribution. **c** Results of the experimental voltage distribution. **d** Error rate between the simulation and experimental voltage distribution results. **e** Histogram of error rate for the voltage distribution. **f** Results of the simulated *E*-field distribution. **g** Results of the experimental *E*-field distribution. **h** Error rate between the simulation and experimental *E*-field distribution results. **i** Histogram of error rate for the E-field distribution

tolerance of 3 mm. Given the higher uncertainty associated with *E*-fields compared to voltage, tolerances of 10% and 5% were applied for *E*-fields, with a distance tolerance of 5 mm.

3 Results

3.1 Voltage distribution and *E*-fields at the center in one dimension

The accuracy of the measured values relative to the actual water phantom was validated using voltage and *E*-field data from simulations as reference values. Figure 2 illustrates the voltage and *E*-field at the center point of the phantom. As the voltage magnitude increased, the measured values at the center point increased proportionally, with an observed error of ± 0.2 V (Fig. 2(a)). At the highest voltage of 50 V, the maximum error observed was within 0.7 V compared to the reference. Figure 2(b) shows the *E*-field values measured with a tolerance of ± 0.05 V/cm, with errors within 0.2 V/cm relative to the reference. Figure 3 presents the simulated and measured voltage and *E*-fields along the centerline of the phantom when a 50 V potential was applied. Figure 3(c) and (d) compares the measured and reference values of voltages and electric fields, revealing errors of less than 0.4 V and 0.04 V/cm, respectively.

3.2 Voltage distribution and E-fields in two dimensions

Figure 4 presents the data for voltage and *E*-fields measured and compared at the + 10 mm from center plane position of the phantom along the *z*-axis. Regarding voltage measurements, 63% of the measurement points exhibited errors within 1%, with a maximum error of 5% and an average error of 0.91%. The *E*-field measurements showed that 68% of the measurement points had errors within 5%, with a maximum error of 49.56% and an average error of 6.57%.

Figure 5 shows the data for voltage and *E*-fields measured and compared at the center plane position of the phantom. For voltage measurements, 46% of the measurement points had errors within 1%, with a maximum error of 13.1%. The *E*-field measurements showed that 48% of the measurement points had errors within 5%, with a maximum error of 46%.

Figure 6 shows the data for voltage and *E*-fields measured and compared at the − 10 mm from the center plane position of the phantom along *z*-axis. Regarding voltage measurements, 56% of the measurement points exhibited errors within 1%, with a maximum error of 8.97% and an average error of 1.31%. The *E*-field measurements showed that 67% of the measurement points had errors within 1%, with a maximum error of 54% and an average error of 5.96%.

3.3 Gamma index and 3D analysis

Figure 7 presents the results of the GI analysis for voltage and *E*-fields at the center plane positions at − 10 mm, 0 mm and + 10 mm from the center. Regarding the voltage distribution, the profiles at + 10 mm, 0 mm, and − 10 mm from the center plane showed gamma passing rates (GPRs) of 100%, 98.89%, and 99.17%, respectively. Figure 7(g), (h) and (i) depicts GI results for *E*-field distributions with a 5%/5 mm criterion applied on the same planes. They show GPRs of 86.98%, 81.16%, and 90.58%, respectively. Figure 8 presents the error rate and gamma analysis results for the voltage and electric field distributions in three dimensions. As shown in the figure, the measured values align closely with the simulated values, demonstrating good agreement.

Table 1 displays the GPRs for voltage and *E*-fields at each profile, considering various gamma criteria. For the voltage, GPRs greater than 98% were observed for profiles at − 20 mm, − 10 mm, 0 mm, + 10 mm, and + 20 mm from the center plane. However, for the *E*-field criteria of 10%/5 mm and 5%/5 mm, the GPRs were relatively lower, with a minimum of 81.16%, compared with GPRs corresponding to the voltage criteria. Table 2 presents the average error rates for the five profiles measured in the experiment, as well as for the 3D voltage and *E*-fields. The average voltage error rate ranged to a maximum of 2.10%, with a 1.06% error rate for the 3D voltage distribution. The *E*-fields exhibited error rates as high as 7.35%, with a 6.65% error rate for 3D E-field distribution.

4 Discussion

E-fields distribute in 3D space and are dependent on the conductivity of objects. Each organ in the body exhibits different conductivity [26]. The distribution of the *E*-fields formed during TTFields therapy varies depending on the position, shape, and number of electrodes, resulting in a complex structure. In the case of 1D and 2D measurements, if the *E*-field distribution is not symmetric, the distribution cannot be accurately confirmed. This fact increases uncertainty about the *E*-fields formed in the region of interest (ROI), and the difference between the calculated *E*-fields and the *E*-fields formed during actual

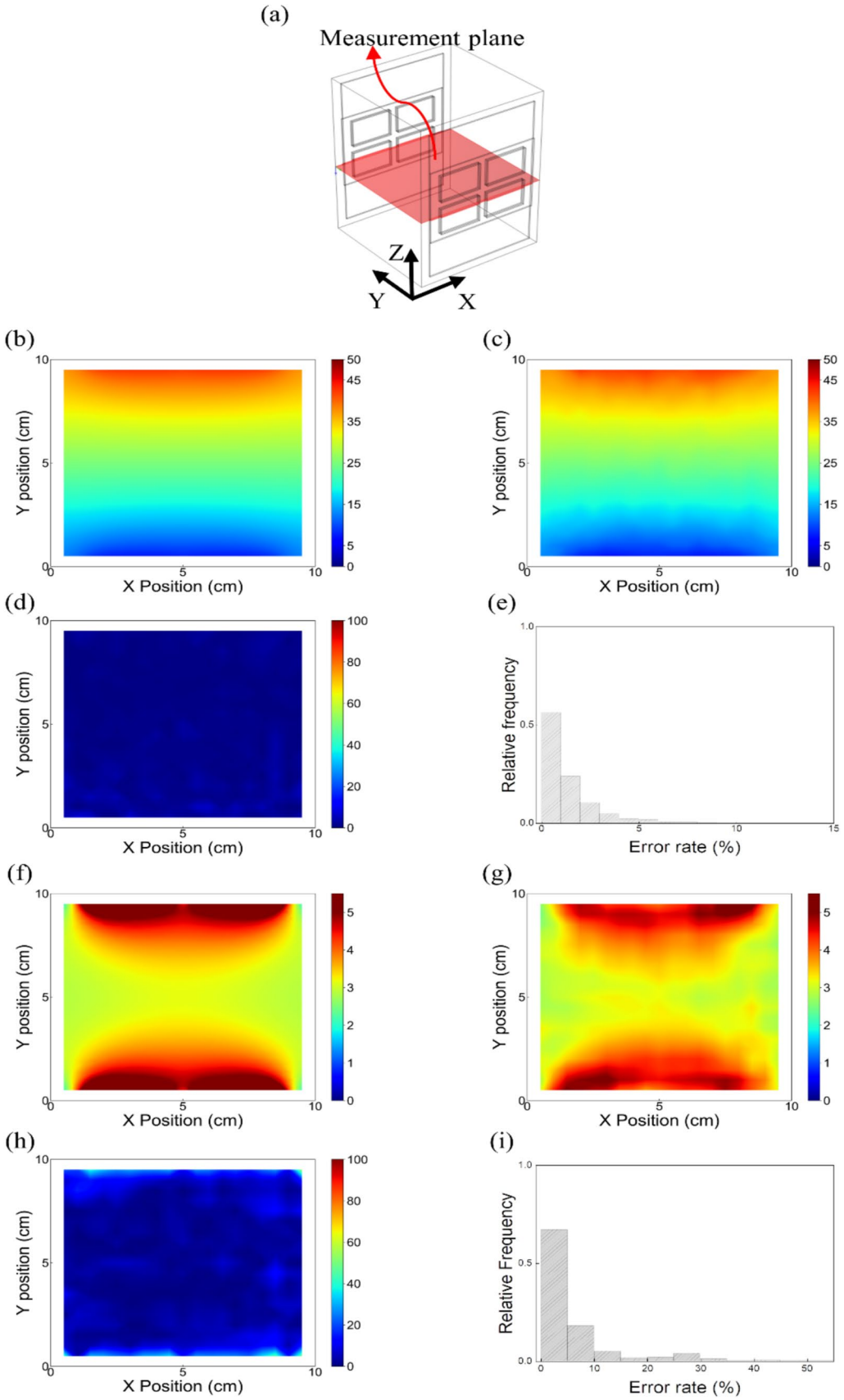
(a)
Measurement plane
Z
Y
X
(b)
Y position (cm)
X Position (cm)
(c)
Y position (cm)
X Position (cm)
(d)
Y position (cm)
X Position (cm)
(e)
Relative frequency
Error rate (%)
(f)
Y position (cm)
X Position (cm)
(g)
Y position (cm)
X Position (cm)
(h)
Y position (cm)
X Position (cm)
(i)
Relative Frequency
Error rate (%)

◂**Fig. 6** Voltage and *E*-field distribution − 10 mm from the center plane. **a** Schematic of the measurement plane. **b** Results of the simulated voltage distribution. **c** Results of the experimental voltage distribution. **d** Error rate between the simulation and experimental voltage distribution results. **e** Histogram of error rate for the voltage distribution. **f** Results of the simulated *E*-field distribution. **g** Results of the experimental *E*-field distribution. **h** Error rate between the simulation and experimental *E*-field distribution results. **i** Histogram of error rate for the E-field distribution

treatment can adversely affect treatment efficacy. By examining the 3D *E*-field distribution, we can confirm the precise magnitude of the *E*-fields formed in the ROI. Therefore, 3D QA is an indispensable procedure that must be carried out to enhance the quality of TTFields treatments.

In previous studies, voltage and electric field measurements for Tumor-Treating Fields (TTFields) quality assurance (QA) were conducted using a single pair of electrodes, which were limited to one-dimensional (1D) or two-dimensional (2D) data along the central axis [21, 22]. Additionally, earlier studies relied on a relatively small number of probes fixed inside the phantom for measurement. Fixed probes can distort the electric field (*E*-field), resulting in discrepancies between the measured field and the actual field generated during treatment. Increasing the number of probes is also challenging, and the low-resolution voltage distribution obtained from such setups restricts the accuracy of measured *E*-field distributions, particularly in areas with rapid field changes, such as those directly beneath the electrodes.

Moreover, the fixed-probe approach in previous studies was confined to 2D QA. However, accurate QA for TTFields requires three-dimensional (3D) assessments. While voltage distribution can be expressed as relative differences compared to the reference potential, making it less dependent on dimensionality, electric field values are inherently dimension-dependent. High-resolution measurements are critical for accurately representing *E*-fields, especially in 3D [25]. Equations (5), (6), and (7) below represent the calculation of electric fields in 1D QA, 2D QA, and 3D QA, respectively.

$$E_{1D} = \frac{\Delta V}{\Delta x} \tag{5}$$

$$E_{2D} = \frac{\Delta V}{\Delta x} + \frac{\Delta V}{\Delta y} \tag{6}$$

$$E_{3D} = \frac{\Delta V}{\Delta x} + \frac{\Delta V}{\Delta y} + \frac{\Delta V}{\Delta z} \tag{7}$$

In the Cartesian coordinate system, 2D QA does not account for variations along the *z*-axis, which leads to discrepancies compared to the actual electric field distribution. Similarly, 1D QA ignores variations along both the *y* and *z*-axes, resulting in even greater inaccuracies. To address these limitations, this study utilized an electrode array combined with a scanning method using a single probe within the water phantom. This approach improved resolution and facilitated accurate 3D QA.

In our analysis, we obtained well-matched results with an error rate of 1.06% and GPR of 99.61% for the measured voltage distribution (Tables 1, 2), indicating precise execution. However, for the *E*-fields, we observed higher error rates and lower passing rates compared with those observed for the voltage. Error may originate from several sources. Unlike previous studies, we adopted a scanning method for moving the probe, increasing uncertainty regarding the probe's position. For the electric fields, in particular, the highest error rate was observed at the high-gradient region, specifically at the center plane, accompanied by a relatively lower GPR. In contrast, in the ± 20 planes with minimal variations, a relatively high GPR was observed under the gamma criteria of 5%/5 mm. However, regions with more rapid changes in the electric fields consistently showed lower GPR values. Another source of error is the resolution of the voltage distribution. The resolution of our experimental results, 1,806 points, accounts for 2.3% of the simulation mesh node count of 75,223 points. In particular, the *z*-axis displacement of 10 mm contributed to this relatively low resolution, resulting in a lower GPR under the gamma criteria of 5%/5 mm. Consequently, the experimental results show lower resolution compared with simulations, leading to increased uncertainty in the calculation of the *E*-fields through the experimental voltage distribution. To resolve these issues, the resolution of experiments could be increased, and the positional errors could be reduced through the use of precise scanning devices, likely yielding more accurate results.

The water phantom used in this work is homogeneous, with uniform conductivity, unlike the various tissues and media comprising the human body, which exhibit conductivities ranging from 0.0245 to 1.4 S/m (at 150 kHz). Therefore, the results obtained from the water phantom might differ from those of actual human tissue. It is necessary to develop phantoms that mimic the diverse conductivities of tissues and media found in the human body. In addition, when a voltage is applied, Joule heating reactions occur, generating heat; however, measuring the temperature distribution in water is challenging. This lack of information about heat complicates the prediction of side effects such as skin burns caused by TTFields. To address all of these issues, further research is needed on inhomogeneous phantoms, particularly solid phantoms, which could be used to create humanoid phantoms. Such phantoms could facilitate more accurate QA for TTFields therapy.

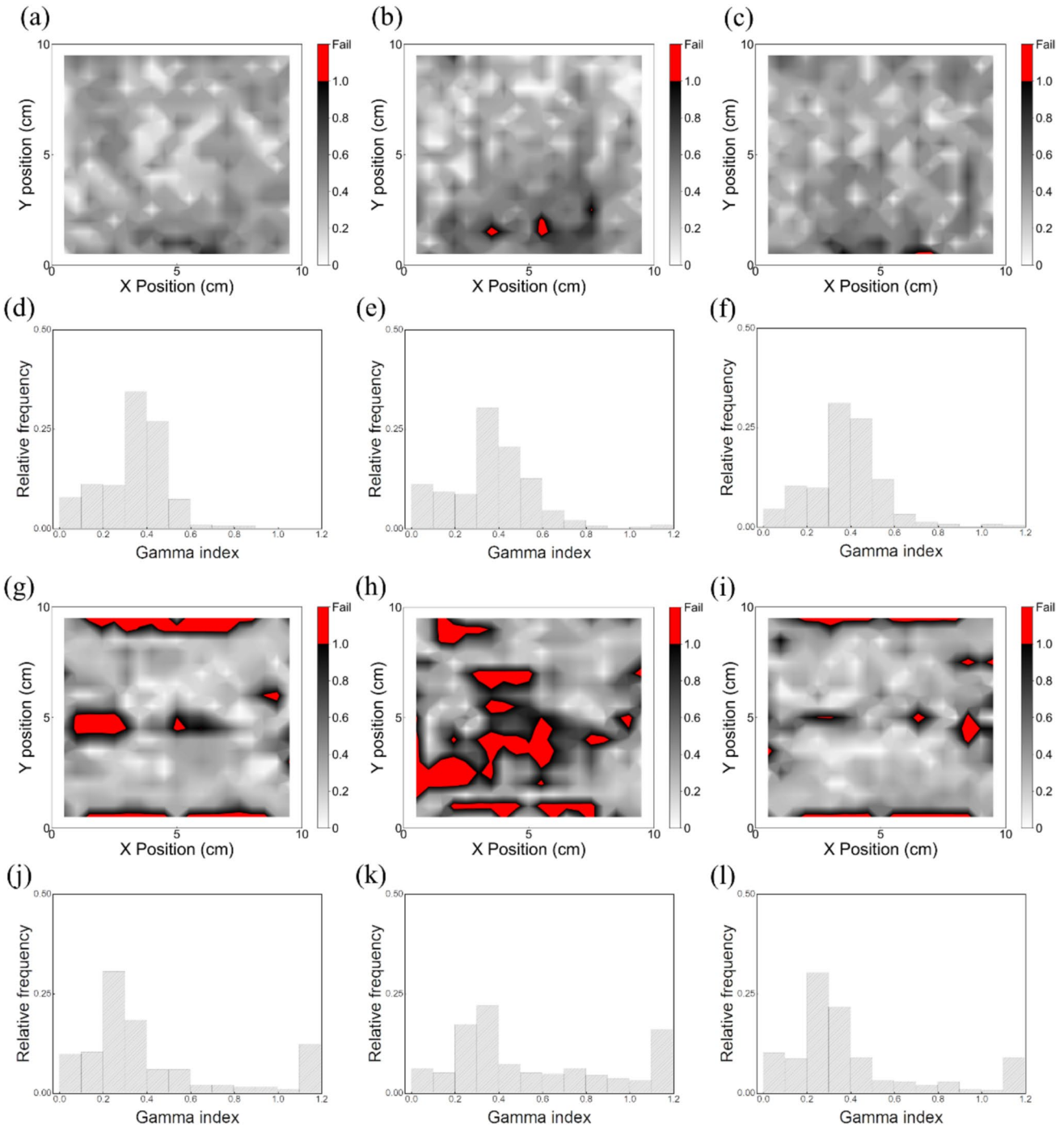

Fig. 7 **a**, **b**, and **c** show the gamma index for the voltage distribution using 3%/3 mm gamma criteria at + 10 mm, 0 mm, and − 10 mm from the center plane, respectively. **d**, **e**, and **f** present the histograms of the gamma analysis results for the voltage distribution at + 10 mm, 0 mm, and − 10 mm from the center plane, respectively. **g**, **h**, and **i** depict the gamma index for the *E*-field distribution using 5%/5 mm gamma criteria at + 10 mm, 0 mm, and − 10 mm from the center plane, respectively. **j**, **k**, and **l** display the histograms of the gamma analysis results for the E-field distribution at the center plane

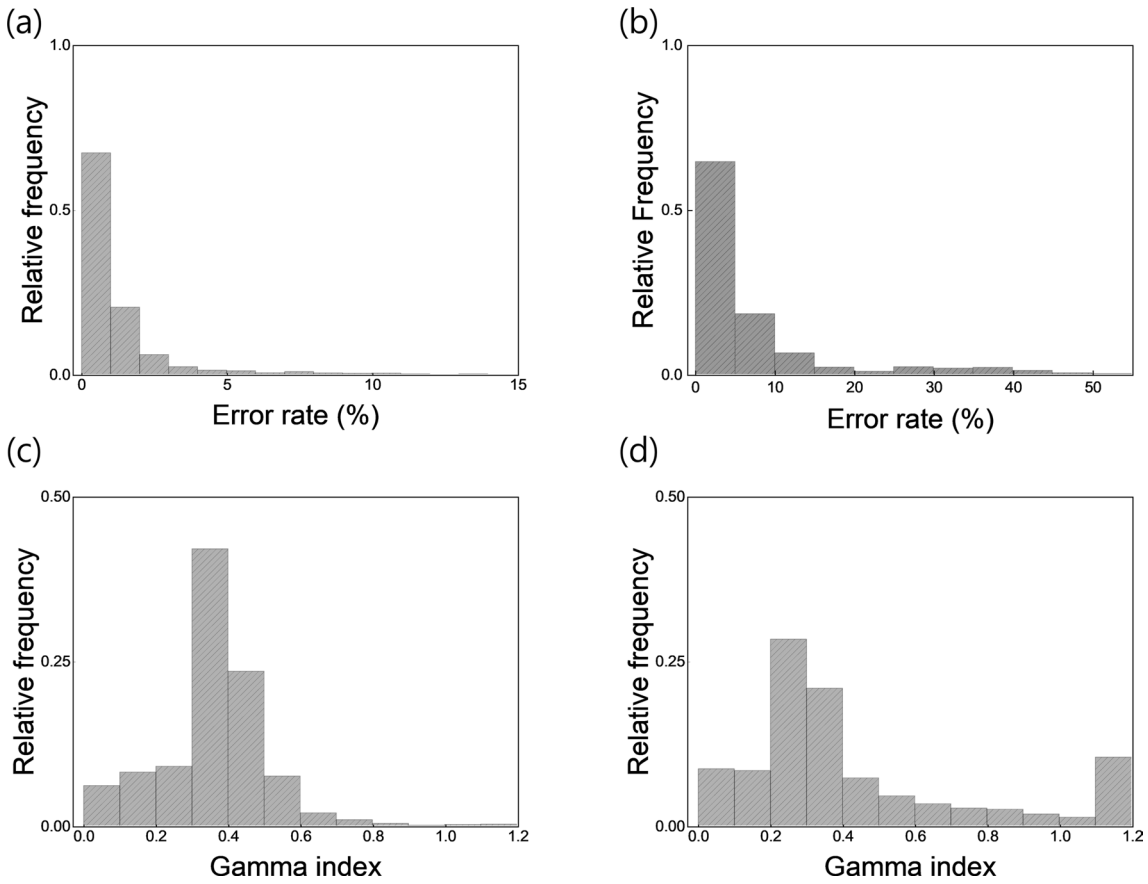

Fig. 8 Error rate and gamma analysis results in three dimensions: **a** Histogram of the error rate for the voltage distribution in three dimensions, **b** Histogram of the error rate for the *E*-field distribution in three dimensions, **c** Histogram of the gamma analysis results for the voltage distribution in three dimensions using 3%/3 mm gamma criteria, and **d** Histogram of the gamma analysis results for the E-field distribution in three dimensions using 5%/5 mm gamma criteria

5 Conclusion

In this study, we investigated the feasibility of a 3D QA system for Tumor-Treating Fields (TTFields) therapy using a water phantom with an electrode array. This method allowed for the verification of 3D *E*-field distributions, providing a relatively accurate assessment of the complex *E*-field patterns generated by the electrode array. The findings of this study are expected to contribute to improving the quality of TTFields therapy through experimental validation of *E*-fields and to facilitate predictions of the therapy's efficacy.

Table 1 Overall gamma index

	Voltage		E-Field	
Profile	5%/3 mm (%)	3%/3 mm (%)	10%/5 mm (%)	5%/5 mm (%)
Center plane + 20 mm	100	100	92.80	91.14
Center plane + 10 mm	100	100	92.80	86.98
Center plane (0 mm)	100	98.89	95.84	81.16
Center plane − 10 mm	100	99.17	93.35	90.58
Center plane − 20 mm	100	100	93.35	91.69
3D (− 20 mm to + 20 mm)	100	99.61	93.63	88.31

Table 2 Overall error rate

Profile	Average voltage error rate (%)	Average E-field error rate (%)
Center plane + 20 mm	0.49	6.73
Center plane + 10 mm	0.91	6.57
Center plane (0 mm)	2.07	7.34
Center plane − 10 mm	1.31	5.97
Center plane − 20 mm	0.60	6.63
3D (− 20 mm to + 20 mm)	1.06	6.65

Acknowledgements This work was supported by a National Research Foundation of Korea (NRF) grant funded by the Korean government (MSIT) (Grant Nos. RS-2023-00253710, NRF-2021R1A2C2008695 and NRF-2022R1A2C1010337) This work was also supported by a Korea Medical Device Development Fund grant funded by the Korean Government (the Ministry of Science and ICT, the Ministry of Trade, Industry and Energy, the Ministry of Health & Welfare, and the Ministry of Food and Drug Safety) (Project No. RS-2023-00254868).

Author contributions Jinyoung Hong :formal analysissoftwarewriting original draftYunhui Jo:investigationwriting - review& editingYongha Gi :softwareWrithing- review & editingGeon oh:InvestigationWrithing- review & editingHyeongjin Lim:softwareWrithing- review & editingYousun Ko:softwareWrithing- review & editingMyonggeun Yoon:ConceptualizationSung Hwan Ahn:Writhing- review & editing

Data availability No datasets were generated or analyzed during the current study.

Declarations

Conflict of interest The authors declare no conflict of interest.

References

1. E.D. Kirson et al., Alternating electric fields arrest cell proliferation in animal tumor models and human brain tumors. Proc. Natl. Acad. Sci. **104**(24), 10152–10157 (2007)
2. E.D. Kirson et al., Disruption of cancer cell replication by alternating electric fields. Can. Res. **64**(9), 3288–3295 (2004)
3. M. Pless, U. Weinberg, Tumor treating fields: concept, evidence and future. Expert Opin. Investig. Drugs **20**(8), 1099–1106 (2011)
4. G. Ceresoli et al., MA12.06 STELLAR–Final results of a phase 2 trial of TTFields with chemotherapy for first-line treatment of malignant pleural mesothelioma. J. Thorac. Oncol. **13**(10), S397–S398 (2018)
5. M. Giladi et al., Alternating electric fields (tumor-treating fields therapy) can improve chemotherapy treatment efficacy in non-small cell lung cancer both in vitro and in vivo. Semin. Oncol. (2014). https://doi.org/10.1053/j.seminoncol.2014.09.006
6. E. Gkika et al., Abstract CT186: HEPANOVA: interim safety analysis from a phase 2 study of Tumor Treating Fields (TTFields, 150 kHz) concomitant with sorafenib in advanced hepatocellular carcinoma (HCC). Cancer Res. **80**(16), CT186–CT186 (2020)
7. F. Rivera et al., Tumor treating fields in combination with gemcitabine or gemcitabine plus nab-paclitaxel in pancreatic cancer: results of the PANOVA phase 2 study. Pancreatology **19**(1), 64–72 (2019)
8. M. Giladi et al., Tumor treating fields (TTFields) delay DNA damage repair following radiation treatment of glioma cells. Radiat. Oncol. **12**(1), 1–13 (2017)
9. Y. Jo et al., Tumor treating fields (TTF) treatment enhances radiation-induced apoptosis in pancreatic cancer cells. Int. J. Radiat. Biol. **96**(12), 1528–1533 (2020)
10. J.-Y. Kim et al., Sorafenib increases tumor treating fields-induced cell death in glioblastoma by inhibiting STAT3. Am. J. Cancer Res. **10**(10), 3475 (2020)
11. M.T. Ballo et al., Correlation of tumor treating fields dosimetry to survival outcomes in newly diagnosed glioblastoma: a large-scale numerical simulation-based analysis of data from the phase 3 EF-14 randomized trial. Int. J. Radiat. Oncol. Biol. Phys. **104**(5), 1106–1113 (2019)
12. X. Li, F. Yang, B. Rubinsky, A theoretical study on the biophysical mechanisms by which tumor treating fields affect tumor cells during mitosis. IEEE Trans. Biomed. Eng. **67**(9), 2594–2602 (2020)
13. G. Oh et al., Correlation between impulse magnitude and inhibition of cell proliferation in alternating electric fields therapy. AIP Adv. (2023). https://doi.org/10.1063/5.0153374
14. G. Oh et al., Potential prognostic factor in alternating electric fields therapy based on absorbed energy in tissue. AIP Adv. (2022). https://doi.org/10.1063/5.0100820
15. P. Dixon, B. O'Sullivan, Radiotherapy quality assurance: time for everyone to take it seriously. Eur. J. Cancer **39**(4), 423–429 (2003)
16. B. Fraass et al., American association of physicists in medicine radiation therapy committee task group 53: quality assurance for clinical radiotherapy treatment planning. Med. Phys. **25**(10), 1773–1829 (1998)
17. F. M. Khan, J.P. Gibbons, Khan's the physics of radiation therapy. 2014: Lippincott Williams & Wilkins
18. E.S.R. Acurio et al., Three-dimensional QA of simultaneous integrated boost radiotherapy treatments by a dose-volume histogram methodology and its comparison with 3D gamma results. Med. Phys. **48**(6), 3208–3215 (2021)
19. D. Low, The importance of 3D dosimetry. J. Phys. Conf. Ser. (2015). https://doi.org/10.1088/1742-6596/573/1/012009
20. M. Rilling et al., Tomographic-based 3D scintillation dosimetry using a three-view plenoptic imaging system. Med. Phys. **47**(8), 3636–3646 (2020)
21. M. Ma, et al., Validation of computational simulation for tumor-treating fields with homogeneous phantom. In: 2022 44th Annual International Conference of the IEEE Engineering in Medicine & Biology Society (EMBC). IEEE (2022)
22. H. Sung et al., Feasibility of a quality assurance system for electromagnetic field therapy. J. Korean Phys. Soc. **81**(11), 1029–1038 (2022)
23. N. Gentilal, Heating of head tissues during TTFields therapy: a computational study. (2018)
24. H. Sung et al., Evaluation of methods for reducing edge current density under electrode arrays for tumor-treating fields therapy. Med. Phys. **49**(7), 4837–4844 (2022)
25. D.J. Griffiths, Introduction to electrodynamics. Am. Assoc. Phys. Teach. (2005). https://doi.org/10.1119/1.4766311
26. S. Gabriel, R. Lau, C. Gabriel, The dielectric properties of biological tissues: II Measurements in the frequency range 10 Hz to 20 GHz. Phys. Med. Biol. **41**(11), 2251 (1996)
27. C. Wenger et al., The electric field distribution in the brain during TTFields therapy and its dependence on tissue dielectric properties and anatomy: a computational study. Phys. Med. Biol. **60**(18), 7339 (2015)

28. D.A. Low et al., A technique for the quantitative evaluation of dose distributions. Med. Phys. **25**(5), 656–661 (1998)